Available online at www.sciencedirect.com
ScienceDirect
Journal of Sound and Vibration 308 (2007) 201–211
JOURNAL OF SOUND AND VIBRATION
www.elsevier.com/locate/jsvi

Characterization of elastic anisotropy of a solid plate using nonlinear Lamb wave approach

Ming-Xi Deng[a,*], Jun Yang[b]

[a]*Department of Physics, Logistics Engineering University, No. 174, Chang Jiang 2 Road, Chongqing 400016, People's Republic of China*
[b]*Institute of Acoustics, Chinese Academy of Science, Beijing 100080, People's Republic of China*

Received 3 August 2006; received in revised form 15 July 2007; accepted 21 July 2007
Available online 4 September 2007

Abstract

A nonlinear Lamb wave approach is presented for characterizing the in-plane elastic anisotropy of a solid plate. The effect of second-harmonic generation in an anisotropic solid plate exists and through this the Lamb waves propagate. When the direction of the Lamb wave propagation in an anisotropic plate changes, the influences of the elastic anisotropy of the plate material on the second-harmonic generation of the Lamb wave propagation have been analyzed. Theoretical analyses show that the effect of second-harmonic generation of the Lamb wave propagation is closely associated with the elastic anisotropy of the solid plate. Based on the theoretical analyses, characterization of the in-plane elastic anisotropy of a given rolled aluminum sheet is experimentally studied. For the different directions of the Lamb wave propagation relative to the rolling direction of the aluminum sheet, the amplitude–frequency curves both of the fundamental waves and the second harmonics of Lamb wave propagation are measured under the condition that the Lamb waves have a strong nonlinearity. It is found that the in-plane elastic anisotropy of the rolled aluminum sheet can clearly affect the efficiency of second-harmonic generation by the Lamb wave propagation. The stress wave factors (SWFs) in acousto-ultrasonic technique are used for reference. Based on the data measured, the normalized SWF curves of the Lamb wave propagation versus the orientation angles relative to the rolling direction of the aluminum sheet are obtained. The results show that the second-harmonic SWF of the Lamb wave propagation varies more sensitively with the orientation angles than does the SWF of the fundamental Lamb wave propagation. It is found that the effect of second-harmonic generation of the Lamb wave propagation can be used to accurately characterize the in-plane elastic anisotropy for the given solid plate.

1. Introduction

Due to the plastic deformation in the rolling manufacture of metal plates, anisotropy of mechanical properties will occur in metal materials. There is in-plane elastic anisotropy in rolled metal plates [1]. Generally speaking, the in-plane elastic anisotropy of a metal plate is associated with microstructural characteristics of the plate material subject to rolled processing. Characterization of the in-plane elastic anisotropy is crucial for discerning the texture of rolled metal plates. For a number of years, study has focused on the measurements of texture of solid plates using a range of ultrasonic modes [2–11]. It is known that the

*Corresponding author. Tel./fax: +86 23 68585624.
E-mail address: dengmx65@yahoo.com (M.-X. Deng).

0022-460X/$ - see front matter © 2007 Elsevier Ltd. All rights reserved.
doi:10.1016/j.jsv.2007.07.029

characteristics of the Lamb wave propagation will be influenced by in-plane elastic anisotropy. Experimental and theoretical studies showed that the Lamb waves could be effectively used for characterizing anisotropic plates [5–11].

To the authors' knowledge, all the measurements of texture or anisotropy using ultrasonic modes are in the linear regime of ultrasonic wave propagation. It is well known that nonlinear ultrasonic measurements can provide more sensitive measures of material properties relevant to microstructures [12–14]. Considering the high sensitivities of nonlinear ultrasonic measurements to the material/structure properties and the existence of strong nonlinearity of the Lamb wave propagation [15–18], the use of the nonlinear effect of the Lamb wave propagation for characterizing the in-plane elastic anisotropy of solid plates will be examined in this paper. It is found that, for characterization of the in-plane elastic anisotropy of solid plates, the effect of second-harmonic generation by the Lamb wave propagation can provide more accurate information than the linear Lamb wave measurements.

2. Theoretical foundations

It is well known that Lamb waves can propagate over long distances and are sensitive to the desired elastic properties of the material. The Lagrangian coordinates (a_1, a_2, a_3) are established for an anisotropic solid plate shown in Fig. 1. Lamb waves are assumed to propagate along the a_3 axis. Through the equations of mechanical boundary conditions, the dispersion relations of the Lamb wave propagation, as well as the corresponding displacement fields, can be determined [19]. The components of the displacement field of a Lamb wave mode (with the frequency f and the order p), propagating in an anisotropic plate (see Fig. 1), can be expressed formally as [19]

$$U_i = U_i^{(f,p)}(a_2)\exp[\mathrm{j}k^{(f,p)}a_3 - \mathrm{j}\omega t], \quad i = 1, 2, 3, \tag{1}$$

where the angular frequency is given by $\omega = 2\pi f$. The subscript i attached to U denotes the components of the displacement field along the a_1, a_2, and a_3 axes. The superscript '(f, p)' attached to U and k denotes the Lamb wave mode with the frequency f and the order p. $k^{(f,\,p)}$ is the a_3-component of wave vectors of partial bulk waves constituting the (f, p) Lamb wave mode. The phase velocity of the (f, p) Lamb wave is given by $c^{(f,\,p)} = \omega/k^{(f,\,p)}$.

The previous work focused on the analyses of second-harmonic generation by the Lamb wave propagation in isotropic solid plates [15–18]. Here we analyze the nonlinear effect of the Lamb wave propagation in anisotropic plates. We assume the elastic constants of the material of the anisotropic plate are defined in the $a_1'\ a_2'\ a_3'$ coordinate system (see Fig. 1). Via the rotation transformation (the rotation angles are, respectively, denoted by γ_1, γ_2 and γ_3), we can get the corresponding elastic constants of the material in the $a_1\ a_2\ a_3$ coordinate system. When the (f, p) Lamb wave travels down the a_3 axis of the structure shown in Fig. 1, the bulk driving force is of double the fundamental frequency in the anisotropic plate because of the convective nonlinearity independent of the material properties and the inherent nonlinearity due to the nonlinear elastic

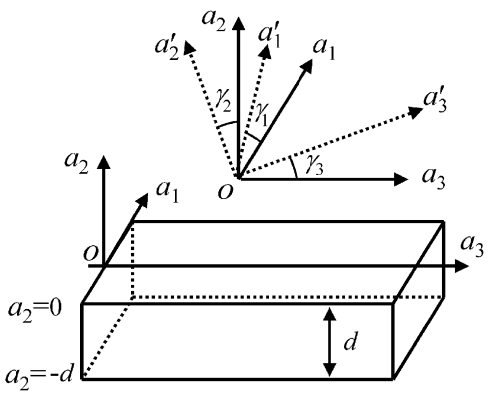

Fig. 1. Schematic representation of an anisotropic solid plate.

properties of the solid [15–17]. The components of the second-order bulk driving force in the interior of the anisotropic plate, denoted by $F_i^{(f,\,p)}(i=1,\,2,\,3)$, are given by [20]

$$F_i^{(f,p)} = \left[C_{ijklmn} + \delta_{km}C_{ijln} + \delta_{im}C_{jnkl} + \delta_{ik}C_{jlmn}\right]\frac{\partial^2 U_k}{\partial a_j \partial a_l}\frac{\partial U_m}{\partial a_n}, \tag{2}$$

where C_{ijkl} and C_{ijklmn} are, respectively, the second- and third-order elastic constants in the $a_1\,a_2\,a_3$ coordinate system, and $i, j, k, l, m, n = 1, 2, 3$. There is the factor $\exp[\mathrm{j}2k^{(f,p)}a_3 - \mathrm{j}2\omega t]$ in $F_i^{(f,\,p)}$. Besides $F_i^{(f,\,p)}$, there are the traction stress tensors of double the fundamental frequency, denoted by $P_{ij}^{(f,\,p)}$ $(i, j = 1, 2, 3)$, at the two surfaces of the anisotropic solid plate [15–17]. $P_{ij}^{(f,\,p)}$ can be written formally as [20]

$$P_{ij}^{(f,p)} = \frac{1}{2}\left[C_{ijklmn} + \delta_{km}C_{ijl\,n} + \delta_{im}C_{jnkl} + \delta_{ik}C_{jlmn}\right]\frac{\partial U_k}{\partial a_l}\frac{\partial U_m}{\partial a_n}. \tag{3}$$

Obviously, $P_{ij}^{(f,\,p)}$ also includes the factor $\exp[\mathrm{j}2k^{(f,p)}a_3 - \mathrm{j}2\omega t]$.

According to a second-order perturbation approximation and a modal analysis approach for waveguide excitation, $F_i^{(f,\,p)}$ and $P_{ij}^{(f,\,p)}$ can be assumed to be a bulk source and a surface source of a series of Double Frequency Lamb waves (abbr. DFLWs), respectively [15–17]. The second-harmonic fields (denoted by $\mathbf{U}^{(2f)}$) generated by $F_i^{(f,\,p)}$ and $P_{ij}^{(f,\,p)}$ can formally be written as follows [15–17,19]:

$$\mathbf{U}^{(2f)} = \sum_q A_q(a_3)\times\mathbf{U}^{(2f,q)}(a_2), \quad U_i^{(2f)} = \sum_q A_q(a_3)\times U_i^{(2f,q)}(a_2), \tag{4}$$

where $U_i^{(2f)}$ $(i=1,\,2,\,3)$ are, respectively, the three components of $\mathbf{U}^{(2f)}$ along the a_1, a_2, and a_3 axes. The displacement field function of the $(2f, q)$ DFLW is denoted by $\mathbf{U}^{(2f,q)}(a_2)$, and $U_i^{(2f,q)}(a_2)$ is the component of $\mathbf{U}^{(2f,q)}(a_2)$ along the a_1, a_2, or a_3 axis. $A_q(a_3)$ is the expansion coefficient of the $(2f, q)$ DFLW.

On the basis of the reciprocity relation and the orthogonality of guided wave modes, the equation governing the expansion coefficient of the $(2f, q)$ DFLW can be written as [15–17]

$$\left[\frac{\partial}{\partial a_3} - \mathrm{j}k^{(2f,q)}\right]A_q(a_3) = \frac{F_S + F_b}{4P_{qq}}\exp[\mathrm{j}2k^{(f,p)}a_3], \tag{5}$$

where $k^{(2f,\,q)}$ is the a_3-component of wave vectors of partial bulk waves constituting the $(2f, q)$ DFLW mode and these are related by $k^{(2f,\,q)} = 2\omega/c^{(2f,\,q)}$, where $c^{(2f,\,q)}$ is the phase velocity of the $(2f, q)$ DFLW. Here,

$$F_b = 2\mathrm{j}\omega\int_{-d}^{0}\sum_{i=1}^{3}[\tilde{U}_i^{(2f,q)}(a_2)\,F_i^{(f,p)}]\mathrm{d}a_2, \tag{6}$$

is the forcing function due to the bulk driving force $F_i^{(f,\,p)}$, and

$$F_S = 2\mathrm{j}\omega\sum_i[\tilde{U}_i^{(2f,q)}(a_2)\hat{a}_i\cdot\mathbf{P}^{(f,p)}\cdot\hat{a}_2 - U_i^{(2f)}\hat{a}_i\cdot\tilde{\mathbf{P}}^{(2f,q)}(a_2)\cdot\hat{a}_2]\Big|_{a_2=-d}^{a_2=0},$$
$$P_{ij}^{(f,p)} = \hat{a}_i\cdot\mathbf{P}^{(f,p)}\cdot\hat{a}_j, \quad P_{ij}^{(2f,q)}(a_2) = \hat{a}_i\cdot\mathbf{P}^{(2f,q)}(a_2)\cdot\hat{a}_j, \tag{7}$$

is the forcing function due to the traction stress tensor $P_{ij}^{(f,\,p)}$. In Eqs. (5)–(7), P_{qq} is the $(2f, q)$ DFLW average power flow, per unit width along the a_1 direction (see Fig. 1). $\hat{a}_i$ is the unit vector along the a_i axis. The sign '$\sim$' denotes the complex conjugate operation for the corresponding physical quantity. $\mathbf{P}^{(2f,\,q)}(a_2)$ is the stress tensor of the $(2f, q)$ DFLW component. The mechanical boundary condition requires that $\mathbf{P}^{(2f,q)}(a_2)\cdot\hat{a}_2$ be zero as $a_2 = 0, -d$ (see Fig. 1). Eq. (7) can further be written as

$$F_S = 2\mathrm{j}\omega\sum_i[\tilde{U}_i^{(2f,q)}(a_2)\hat{a}_i\cdot\mathbf{P}^{(f,p)}\cdot\hat{a}_2]\Big|_{a_2=-d}^{a_2=0}. \tag{8}$$

The position of excitation source for the (f, p) Lamb wave is assumed to be at $a_3 = 0$. The initial condition for the $(2f, q)$ DFLW generation requires that $A_q(a_3)$ be zero when $a_3 = 0$. $A_q(a_3)$ can formally be derived

from Eq. (5) as follows [15]:

$$A_q(a_3) = \frac{(F_S + F_b)}{4P_{qq}/d} \frac{\sin[D k^{(f,p)} a_3]}{D k^{(f,p)} d} \exp[\mathrm{j}k^{(2f,q)} a_3 + \mathrm{j}Dk^{(f,p)} a_3], \tag{9}$$

where $D = [c^{(2f,\ q)} - c^{(f,\ p)}]/c^{(2f,\ q)}$ is the relative difference of phase velocity between the (f, p) Lamb wave and the ($2f$, q) DFLW. When $D = 0$ or $D \approx 0$, the amplitude of the ($2f$, q) DFLW component will grow with propagation distance. When $D \neq 0$, there is a beat effect for the amplitudes of the ($2f$, q) DFLWs with propagation distance [15]. This result is the same as that when the fundamental Lamb waves propagate in an isotropic solid plate. It should be noted that only the propagation modes of Lamb waves are considered, and the evanescent wave modes are neglected.

For a given direction of the Lamb wave propagation (being consistent with the a_3 axis), such as the rolling direction of a rolled metal sheet, the (f, p) Lamb wave mode can be selectively generated to ensure $D = 0$ or $D \approx 0$ (namely $c^{(f,\ p)} = c^{(2f,\ q)}$ or $c^{(f,\ p)} \approx c^{(2f,\ q)}$). The ($2f$, q) DFLW component will grow with propagation distance, and the obvious second-harmonic signals of the Lamb wave propagation may be observed. When the direction of the (f, p) Lamb wave propagation (being consistent with the a_3 axis) changes, due to the elastic anisotropy of the solid plate, the second-harmonic signals of the (f, p) Lamb waves will be influenced by the following aspects. First, F_S and F_b in Eq. (9) are associated with the second- and third-order elastic constants of the material of the anisotropic plate in the a_1 a_2 a_3 coordinate system [namely C_{ijkl} and C_{ijklmn} in Eqs. (2) and (3)]. This will lead to changes in the magnitude of $A_q(a_3)$ when the direction of the Lamb wave propagation changes (namely the rotation angles in Fig. 1 change). Second, the elastic anisotropy of the solid plate will influence the dispersion relations of Lamb waves. The condition $c^{(f,\ p)} = c^{(2f,\ q)}$ or $c^{(f,\ p)} \approx c^{(2f,\ q)}$ may not now be satisfied exactly for the other directions of Lamb wave propagation. This will remarkably influence the efficiency of second-harmonic generation by the (f, p) Lamb wave propagation [15]. When there is a clear difference between $c^{(f,\ p)}$ and $c^{(2f,\ p)}$, the ($2f$, q) DFLW component may not have a cumulative growth effect with propagation distance. For this case, second-harmonic signals cannot be detected effectively. Further, the elastic anisotropy of the plate material can provide different acoustic field features for the (f, p) Lamb wave propagating in different directions. This will also influence the magnitude of $A_q(a_3)$ because F_S and F_b in Eq. (9) are proportional to the square of the amplitude of the (f, p) Lamb wave [20]. The above analyses indicate that the elastic anisotropy of a solid plate can effectively influence the efficiency of second-harmonic generation by Lamb wave propagation.

3. Experimental examinations

The anisotropic plate considered here is a rolled aluminum sheet of 1.80 mm thickness. The elastic anisotropy of the material of the rolled aluminum sheet may be assumed to be a slight departure from the elastic isotropy of the aluminum [1]. For simplicity, the material of the rolled aluminum sheet is thought of to be isotropic when we compute the dispersion curves of the Lamb wave propagation. The dispersion curves for the fundamental Lamb waves and the symmetric DFLWs are shown in Fig. 2 for an isotropic aluminum sheet of 1.80 mm thickness [15].

Liquid wedge transducers are used to generate the fundamental Lamb waves, and to detect the fundamental waves and the second harmonics of Lamb wave propagation at the surface of the rolled aluminum sheet. The oblique angle β of the liquid wedge transducers is given by $\sin\beta = c_L/c^{(f,\ p)}$, where c_L is the longitudinal wave velocity of the liquid (silicon oil, $c_L = 1.080$ MHz mm). The oblique angle of the liquid wedges is 7.5°. The phase velocity of the fundamental Lamb wave to be generated ($c^{(f,\ p)} = c_L/\sin\beta = 8.274$ MHz mm) is determined by the dashed line H in Fig. 2. It can be found that the intersection between the A_2 (S_2) Lamb wave dispersion curve and the dashed line N is very close to the one between the symmetric DFLW dispersion curve and the line N. This means that there is a relationship $c^{(f,p)} \approx c^{(2f,Q_0)}$ ($p = S_2$, A_2) at the frequency given by the dashed line N in Fig. 2. The intersections between the dashed line N and the dispersion curves of the symmetric DFLWs (namely the points Q_0, Q_1, Q_2, Q_3, etc.) denote the DFLW components constituting the fields of second harmonics by the A_2 and S_2 Lamb wave propagation, whose phase velocity is determined by the dashed line H in Fig. 2 [15–17]. According to the expression of the DFLW expansion coefficient shown in

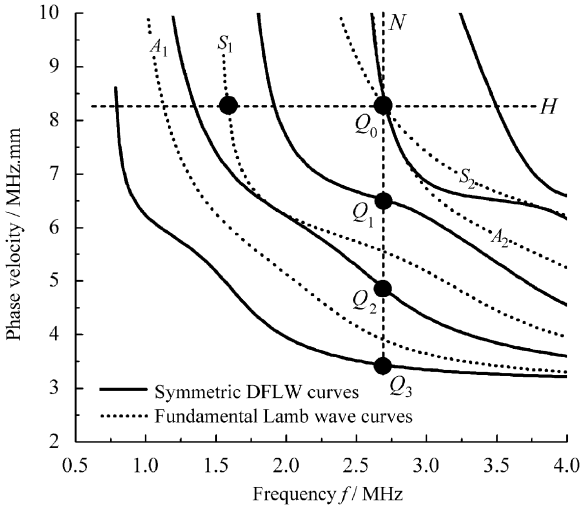

Fig. 2. Dispersion curves of Lamb waves.

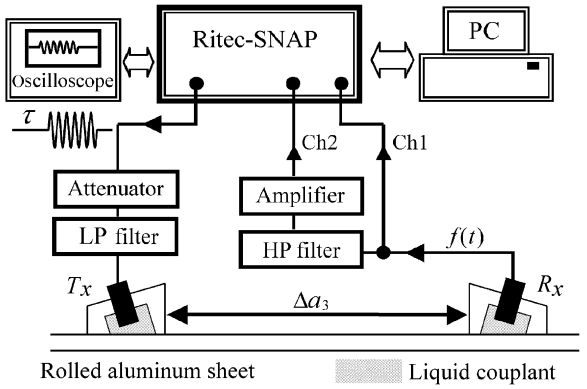

Fig. 3. Block diagram of the experimental setup for Lamb waves.

Eq. (9), the Q_0 DFLW component may have a cumulative growth effect and the contribution of the other DFLW components (namely the points Q_1, Q_2, Q_3, etc.) to $\mathbf{U}^{(2f)}$ may be neglected.

Fig. 3 illustrates the experimental setup for Lamb waves. The liquid wedge transducers Tx and Rx with the same oblique angles (7.5°) are used to generate the fundamental Lamb waves, and to detect the fundamental- and double-frequency signals of the Lamb wave propagation. The central frequencies of the longitudinal wave transducers Tx and Rx are, respectively, 2 and 4 MHz, and the effective diameters of Tx and Rx are 20 mm. The cutoff frequencies for the low pass (LP) and high pass (HP) filters are, respectively, around 3.3 and 4.7 MHz. It should be noted that the liquid couplant (silicon oil) is used to ensure that the acoustic coupling conditions between the transducers and the aluminum sheet are kept the same for all the measurements.

The transmitting transducer Tx driven by tone-burst voltages (with the carrier frequency f and the burst duration τ) generates time-domain pulses of Lamb waves (see Fig. 3). The LP filter is used to eliminate the higher harmonic frequency components of the tone-burst voltages applied to Tx. The Ritec-SNAP system is used to generate tone-burst voltages for excitation of the transducer Tx, and to perform the signal receiving and processing for the primary and secondary waves of the Lamb wave propagation in the rolled aluminum sheet [18,21]. The ultrasonic signal can be assumed to be a time-domain burst $f(t)$, modulated by a term $A_r(t)$. $f(t)$ can formally be written as $f(t) = A_r(t)\sin(2\pi f_r t + \varphi_r)$, where φ_r represents the phase shift in the transducer and sample including the effect of the acoustic transit time [22]. The carrier frequency f_r of $f(t)$ may be f

(i.e. fundamental wave) or $2f$ (i.e. second harmonic). The Ritec-SNAP system produces the two integration signals associated with $A_r(t)$ [18,22],

$$I_1 = R\cos\varphi_r \int_{t_1}^{t_2} A_r(t)\mathrm{d}t, \quad I_2 = R\sin\varphi_r \int_{t_1}^{t_2} A_r(t)\mathrm{d}t, \tag{10}$$

where $A_r(t)$ should be wholly located between t_1 and t_2, and R is a constant associated with the parameter setups of the Ritec-SNAP system. The amplitude of the sine wave $\sin(2\pi f_r t + \varphi_r)$ can be given by [18,22]

$$\bar{A}_r(f_r) = \int_{t_1}^{t_2} A_r(t)\mathrm{d}t = R^{-1}\sqrt{I_1^2 + I_2^2}. \tag{11}$$

When $f_r = f$, the fundamental Lamb waves can be thought of as the carrier of $f(t)$. $\bar{A}_r(f)$ denotes the resultant amplitude of coherent superpositions of the multimode Lamb waves (being regarded as continuous waves) [18]. When $f_r = 2f$, the resultant amplitude of second harmonics, $\bar{A}_r(2f)$, can be used to characterize the efficiency of second-harmonic generation by the propagation of the fundamental Lamb wave pulses [18].

When a tone burst (produced by the Ritec-SNAP system) is used to generate the transmitting wedge transducer (Tx), the Lamb wave propagation occurs in the rolled aluminum sheet. The signals both of primary waves and second harmonics are simultaneously detected by the receiving wedge transducer (Rx). Via the Ritec-SNAP signal receiving and processing system, the amplitude–frequency curves for the primary waves and second harmonics of the Lamb wave propagation are shown in Fig. 4, where the direction of the Lamb wave propagation (namely the a_3-axis in Fig. 1) is along the rolling direction of the rolled aluminum sheet, and the separation between Tx and Rx (i.e., Δa_3) is 13 cm. The direct path signal of the tone burst for excitation of the transmitting wedge transducer Tx cannot be observed in the receiving signal (i.e., $f(t)$) between the lower and upper limits of the integral $\int_{t_1}^{t_2} A_r(t)\mathrm{d}t$ (namely t_1 and t_2). Near the frequencies $f = 1.6$ and 2.5 MHz, the fundamental S_1, A_2, and S_2 Lamb waves can be observed (see Figs. 2 and 4). In the immediate vicinity of $f = 2.5$ MHz (theoretical prediction, $f = 2.65$ MHz, given by the dashed line N in Fig. 2), a clear second-harmonic response is detected. This clear response should be attributed to the strong nonlinearity of Lamb wave propagation. In the measurements of frequency scans, both the duration and the amplitude of tone-burst voltages applied to Tx are kept unchanged.

We change the distance between Tx and Rx (Δa_3 varies from 7 cm to 16 cm, and the change step is 1 cm), and perform similar frequency-swept measurements for $\bar{A}_r(f)$ and $\bar{A}_r(2f)$ as those whose results are shown in Fig. 4 (the parameter setups for the experimental system are kept unchanged, and Lamb waves propagate along the rolling direction of the rolled aluminum sheet). Near the driving frequency given by the dashed line

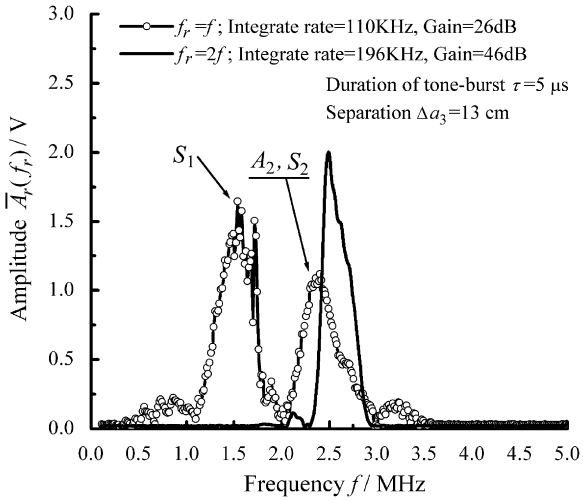

Fig. 4. Amplitude–frequency curves for the fundamental- and double-frequency signals of the Lamb wave propagation along the rolling direction of the rolled aluminum sheet.

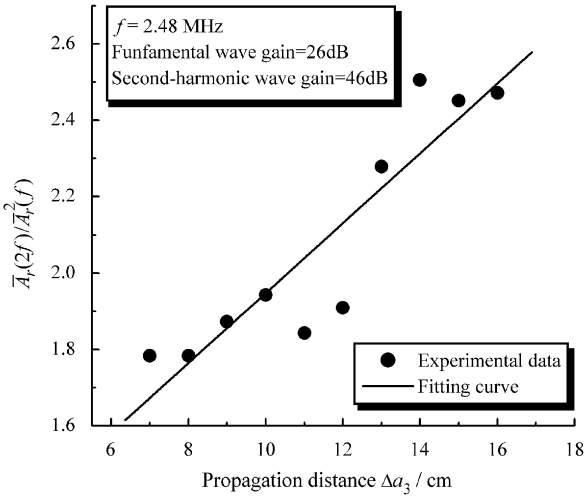

Fig. 5. Curve of $\bar{A}_r(2f)/\bar{A}_r^2(f)$ versus Δa_3.

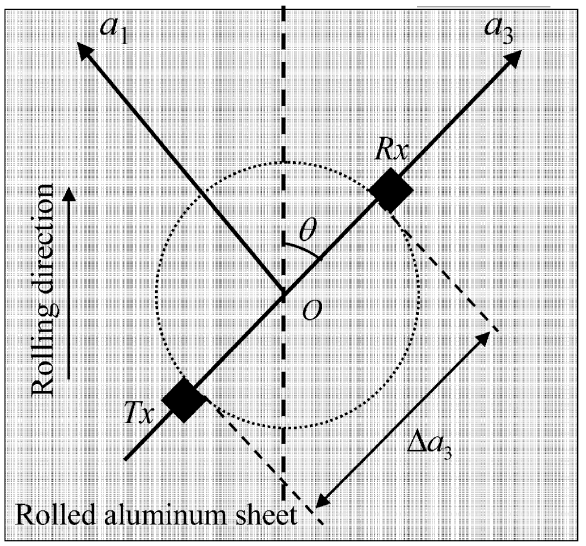

Fig. 6. Arrangement planform of the transducers and the rolled aluminum sheet.

N in Fig. 2, the curve of $\bar{A}_r(2f)/\bar{A}_r^2(f)$ is shown as a function of propagation distance Δa_3, in Fig. 5 [18]. It can readily be observed that the amplitudes of the second harmonics of Lamb waves propagating along the rolling direction of the aluminum sheet grow with propagation distance near the driving frequency given by the dashed line N in Fig. 2, where the condition $c^{(f,p)} \approx c^{(2f,Q_0)}$ $(p = S_2, A_2)$ is satisfied.

Next, we experimentally examine the influence of the in-plane elastic anisotropy of the rolled aluminum sheet on the effect of second-harmonic generation by the lamb wave propagation. The arrangement planform of the transducers and the rolled aluminum sheet is shown in Fig. 6, where θ is the orientation angle of the a_3 axis (namely the direction of Lamb wave propagation) relative to the rolling direction. We change the orientation angle θ, and perform the similar frequency-swept measurements for $\bar{A}_r(f)$ and $\bar{A}_r(2f)$ as those whose results are shown in Fig. 4. In all the measurements, the separation between Tx and Rx (i.e., Δa_3) is always 11 cm, and the parameter setups for the experimental system are kept unchanged. The change step of the orientation angle θ is 15°. It should be pointed out that the liquid couplant (silicon oil) between the wedge transducers and the aluminum sheet (see Fig. 3) can ensure the acoustic coupling condition to be almost the

same for all the measurements. For quantifying the repeatability of the proposed measurements, at the same position of the wedge transducers *Tx* and *Rx* (see Fig. 6), the repeated measurements are carried out three times. In the process of the repeated measurements for $\bar{A}_r(f_r)$ ($f_r = f$, $2f$), the wedge transducers (*Tx* and *Rx*) are removed and then re-located again at the same positions for the next measurement. Fig. 7 presents the repeated measurement curves of $\bar{A}_r(f_r)$ for $\theta = 0^\circ$, 15°, 45°, 75°, 90°, 105°, 135° and 165°. It can readily be found that $\bar{A}_r(2f)$ is sensitive to changes in the orientation angle θ. For considering the influence of the driving frequency f on $\bar{A}_r(f_r)$, a parameter is given by [21,23]

$$\mathrm{SWF}(f_r) = \int_{f_1}^{f_2} [\bar{A}_r(f_r)]^2 \mathrm{d}f, \tag{12}$$

where $f_r = f$ or $2f$; f_1 and f_2 are 0.1 and 4 MHz, respectively. Considering the fact that the Lamb wave modes are dominant in the measurements of frequency scans, and the concept of stress wave factors (SWFs) in acousto-ultrasonic technique [23], SWF(f) and SWF($2f$) are termed SWFs of the fundamental waves and the second harmonics of Lamb wave propagation, respectively. The features of Lamb wave propagation

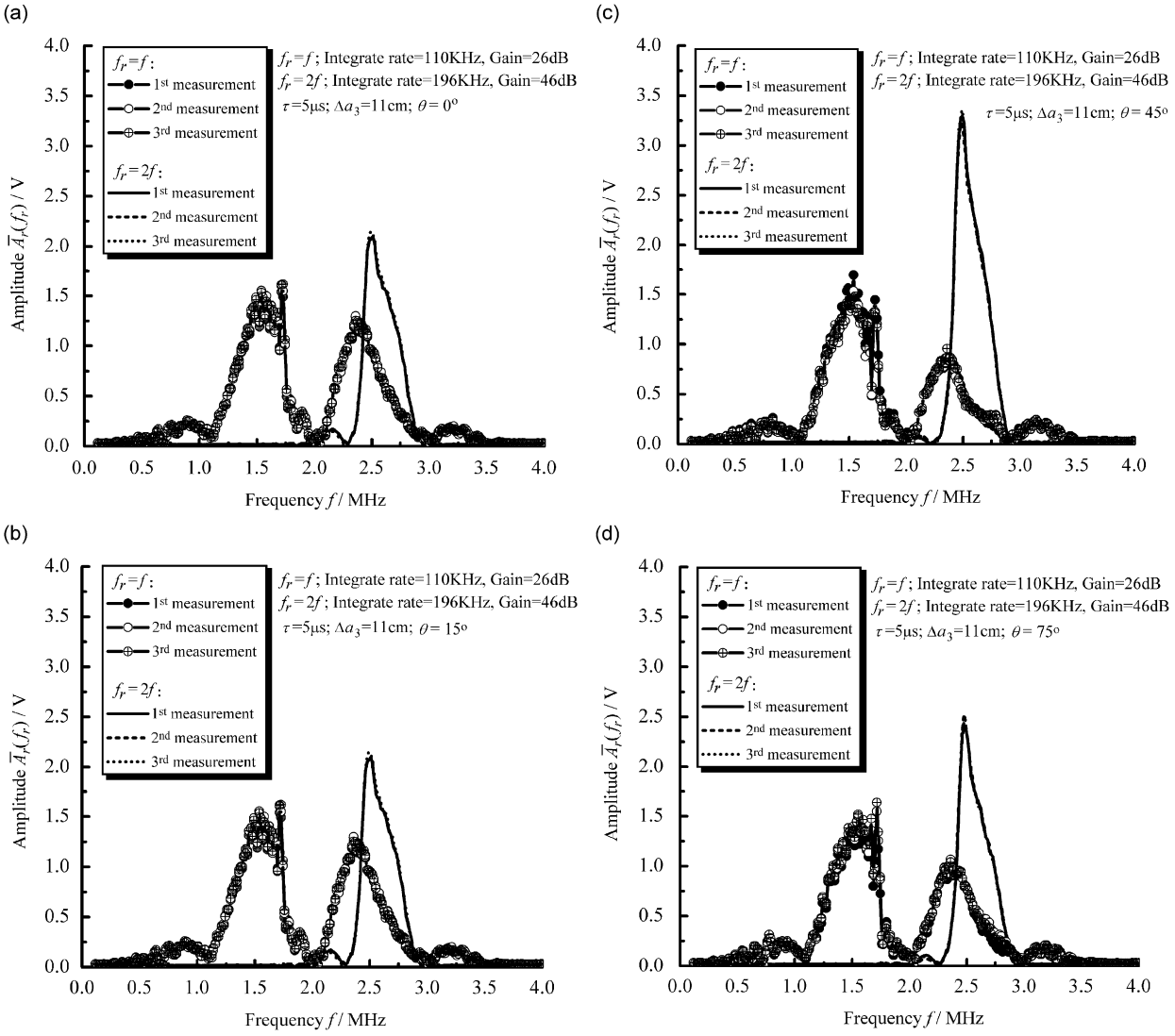

Fig. 7. Amplitude–frequency curves for the fundamental- and double-frequency signals of the Lamb wave propagation with respect to the different orientation angles; (a) $\theta = 0^\circ$; (b) $\theta = 15^\circ$; (c) $\theta = 45^\circ$; (d) $\theta = 75^\circ$; (e) $\theta = 90^\circ$; (f) $\theta = 105^\circ$; (g) $\theta = 135^\circ$; (h) $\theta = 165^\circ$.

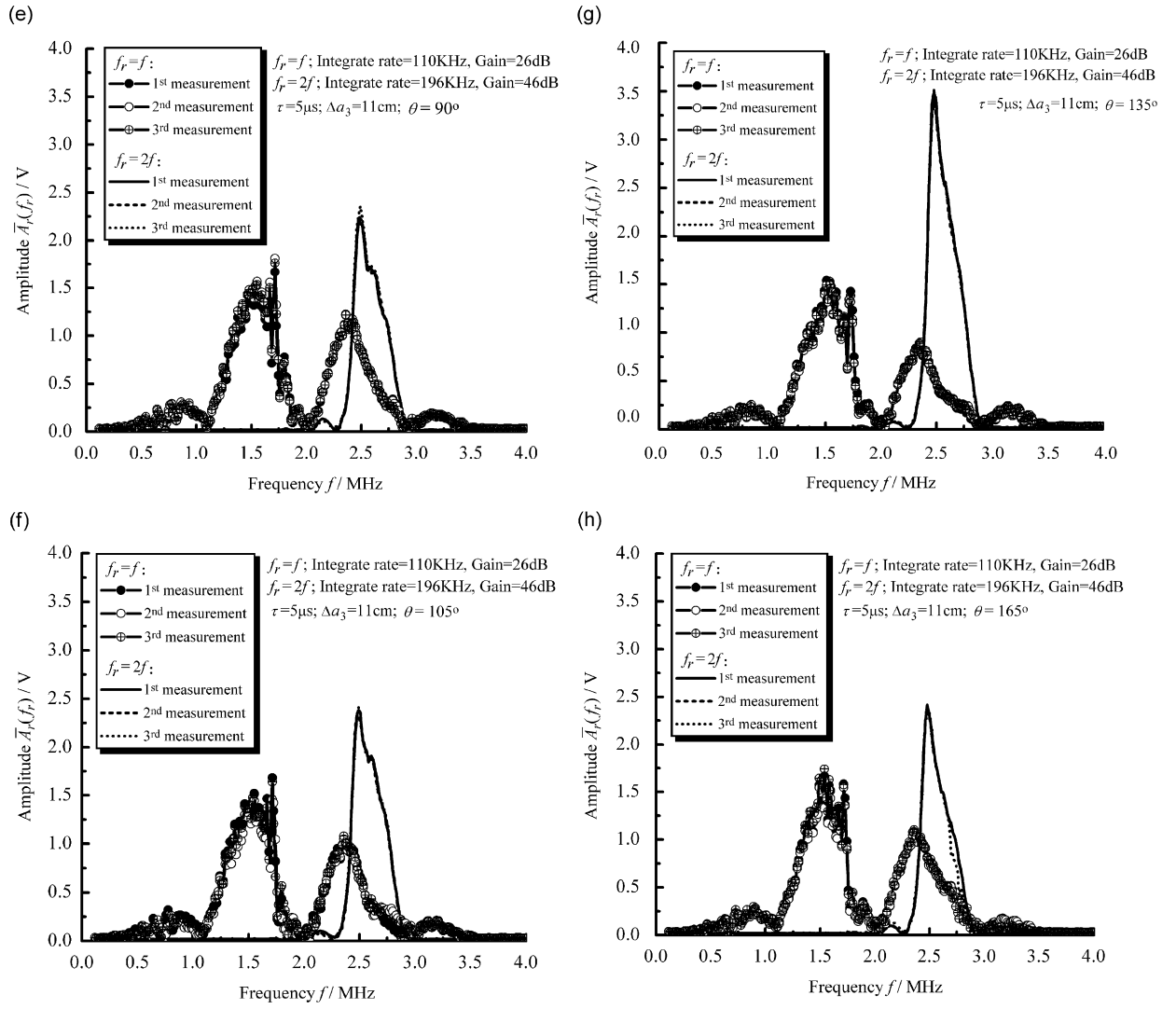

Fig. 7. (*Continued*)

associated with the in-plane elastic anisotropy of the rolled aluminum sheet can be reflected by the parameter SWF(f_r). It is rational to use SWF(f_r) to characterize the in-plane elastic anisotropy of the rolled aluminum sheet. Based on the curves of the repeated measurements for $\bar{A}_r(f_r)$, the average values of SWF(f_r), defined in Eq. (12), can be calculated for different orientation angles. It is found that the relative error of the repeated measurements for SWF(f_r) is below 6%. For the case $\theta = 0^\circ$, the average values of SWF(f) and SWF($2f$) are, respectively, 1.23 and 0.96 V^2 MHz. Fig. 8 shows the normalized curves of the averaged SWF(f) and SWF($2f$) (relative to the average values of SWF(f) and SWF($2f$) at $\theta = 0^\circ$, respectively) versus the orientation angle θ. It can readily be found that the normalized curve of SWF($2f$) is very sensitive to the orientation angle θ. This result is consistent with the theoretical prediction presented in the last paragraph of Section 2.

It should be noted that the efficiency of second-harmonic generation by Lamb wave propagation is not only dependent on the displacement fields of the fundamental Lamb wave propagation, but also on the third-order elastic constants of the material of the anisotropic plate and the relative difference between $c^{(f,\,p)}$ and $c^{(2f,\,p)}$ [15]. Thus, the change tendency of SWF($2f$) may be different from that of SWF(f) [see Fig. 8].

The above preliminary experimental investigations show that the effect of second-harmonic generation by the Lamb wave propagation and SWF($2f$) are very sensitive to the in-plane elastic anisotropy of the rolled

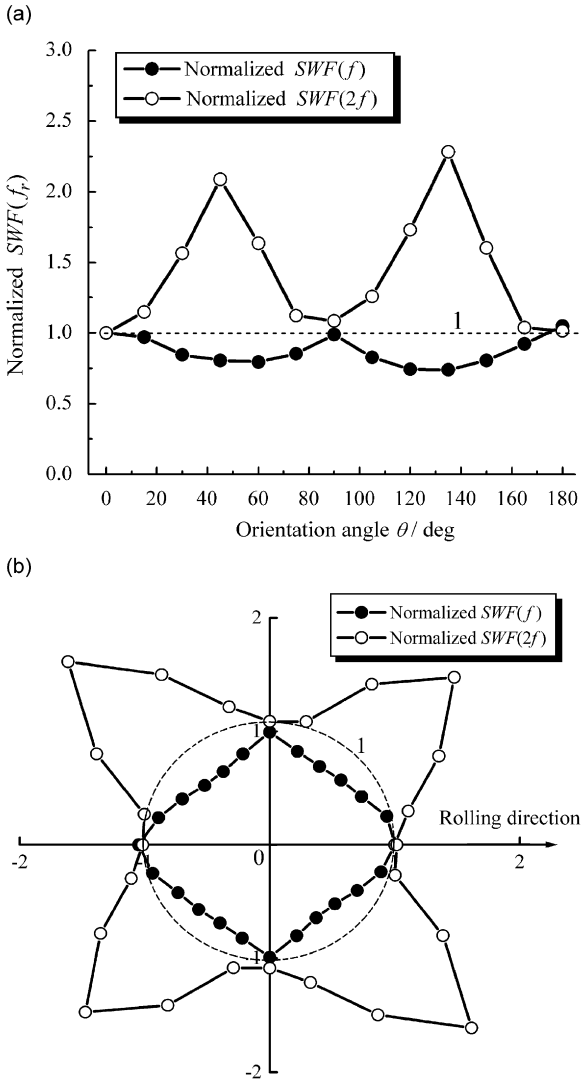

Fig. 8. Normalized curves of SWF(f_r) versus the orientation angle θ; (a) SWF(f_r)-θ rectangular coordinate representation; (b) SWF(f_r)-θ polar coordinate representation.

aluminum sheet. The nonlinear Lamb wave measurements are more sensitive to the in-plane elastic anisotropy than the linear Lamb wave measurements. The experimental results provide a potential that the in-plane elastic anisotropy of solid plates can be accurately evaluated with SWF($2f$).

4. Conclusions

An approach using the nonlinear effect of the Lamb wave propagation to characterize the in-plane elastic anisotropy of a solid plate is proposed. Using a second-order perturbation approximation and a modal analysis approach for waveguide excitation, the formal solution of the second harmonics of the Lamb wave propagation in an anisotropic solid plate has been obtained. When the direction of the Lamb wave propagation changes, the influences of the elastic anisotropy of a solid plate on the second-harmonic generation of the Lamb wave propagation have been analyzed. Theoretical analyses indicate that the effect of second-harmonic generation of the Lamb wave propagation is closely associated with the anisotropy of mechanical properties of a solid plate. When the direction of the Lamb wave propagation in the given rolled aluminum sheet changes, the amplitude–frequency

curves both of the fundamental waves and the second harmonics of the Lamb wave propagation are measured under the condition that Lamb waves have a strong nonlinearity. The normalized curves of the SWFs of the Lamb wave propagation versus the orientation angle relative to the rolling direction are obtained. The preliminary experimental results show that the effect of second-harmonic generation by the Lamb wave propagation is very sensitive to the in-plane elastic anisotropy of the rolled aluminum sheet. Especially, the normalized curve of the second-harmonic SWF of Lamb wave propagation versus the orientation angle offers an accurate approach for evaluating the in-plane elastic anisotropy of the rolled aluminum sheet. This paper provides a potential for accurate characterization of the in-plane elastic anisotropy of solid plates.

Acknowledgments

This work was supported by the NSFC under Grant no. 10674180. Also, this work was partially supported by the CAS Hundreds-Talent Program.

References

[1] V. Eyraud, M.H. Nadal, C. Gondard, Texture measurement of shaped material by impulse acoustic microscopy, *Ultrasonics* 38 (2000) 438–442.
[2] R.B. Thompson, S.S. Lee, J.F. Smith, Relative anisotropies of plane waves and guided modes in thin orthorhombic plates: implication for texture characterization, *Ultrasonics* 25 (1987) 133–137.
[3] R.B. Thompson, Ultrasonic characterization of the texture and formability of rolled metal sheets, *Materials Evaluation* 51 (1993) 1162–1165.
[4] I.Y. Solodov, R. Stoessel, G. Busse, Material characterization and NDE using focused slanted transmission mode of air-coupled ultrasound, *Research in Nondestructive Evaluation* 15 (2004) 65–85.
[5] D.E. Chimenti, A.H. Nayfeh, Leaky lamb waves in fibrous composite laminates, *Journal of Applied Physics* 58 (1985) 4531–4538.
[6] A. Anderson, R.B. Thompson, R. Bolingbroke, Ultrasonic characterization of the texture of aluminum alloys, *Materials Science Forum* 157 (1994) 295–300.
[7] W. Yang, T. Kundu, Efficient use of lamb waves to characterize multilayered anisotropic plates, in: *Wave Propagation and Emerging Technologies*, Vol. 188, American Society of Mechanical Engineers, Applied Mechanics Division, AMD, 1994, pp. 109–120, *Proceedings of the 1994 International Mechanical Engineering Congress and Exposition*, November 6–11, 1994, Chicago, IL, USA.
[8] Y. Li Y, R.B. Thompson, Effects of dispersion on the inference of metal texture from S0 plate mode measurements. Part I. Evaluation of dispersion correction methods, *Journal of the Acoustic Society of America* 91 (1992) 1298–1309.
[9] J.L. Rose, A baseline and vision of ultrasonic guided wave inspection potential, *Journal of Press Vessel Technology* 124 (2002) 273–282.
[10] J.H. Cantrell, Fundamental and Applications of nonlinear ultrasonic NDE, in: Ultrasonic Nondestructive Evaluation: Engineering and Biological Material Characterization, CRC Press, Boca Raton, FL, 2004.
[11] W. Yang, T. Kundu, Guided waves in multilayered anisotropic plates for internal defect detection, *ASCE Journal of Engineering Mechanics* 124 (1998) 311–318.
[12] Y. Belyaeva, V.V. Zaitsev, Nonlinear elastic properties of microinhomogeneous hierarchically structured materials, *Acoustical Physics* 43 (1997) 510–515.
[13] W.T. Yost, J.H. Cantrell, Materials characterization using acoustic nonlinearity parameters and harmonic generation, *Review of Progress in QNDE* 9B (1990) 1669–1676.
[14] L. Adler, P.B. Nagy, Second order nonlinearities and their application in NDE, *Review of Progress in QNDE* 10B (1991) 1813–1820.
[15] M.X. Deng, Analyses of second-harmonic generation of Lamb modes using modal analysis approach, *Journal of Applied Physics* 94 (2003) 4152–4159.
[16] W.J. Lima, M.F. Hamilton, Finite-amplitude waves in isotropic elastic plates, *Journal of Sound and Vibration* 265 (2003) 819–839.
[17] W.J. Lima, M.F. Hamilton, Finite amplitude waves in isotropic elastic waveguides with arbitrary constant cross-sectional area, *Wave Motion* 41 (2005) 1–11.
[18] M.X. Deng, P. Wang, X.F. Lv, Experimental observation of cumulative second-harmonic generation of Lamb-wave propagation in an elastic plate, *Journal of Physics D—Applied Physics* 38 (2005) 344–353.
[19] B.A. Auld, *Acoustic Fields and Waves in Solids*, Wiley, New York, 1973.
[20] M.F. Hamliton, D.T. Blackstock, *Nonlinear Acoustics*, Academic, New York, 1998.
[21] M.X. Deng, P. Wang, X. Lv, Influences of interfacial properties on second-harmonic generation of Lamb waves propagating in layered planar structures, *Journal of Physics D—Applied Physics* 39 (2006) 3018–3025.
[22] Operation manual of Ritec advanced measurement system, Model SNAP-0.25-7, RITEC, USA, 2000.
[23] A. Vary, K.J. Bowles, An ultrasonic-acoustic techniques for nondestructive evaluation of fiber composite quality, *Polymer Engineering Science* 19 (1979) 373–376.